Proceedings of the PHOTON-2017 Conference, Geneva, Switzerland, 22 – 26 May 2017, edited by David d'Enterria, Albert de Roeck and Michelangelo Mangano, CERN Proceedings, Vol. 1/2018, CERN-Proceedings-2018-001 (CERN, Geneva, 2018)

Very forward photon production in proton-proton collisions at $\sqrt{s}$ = 13 TeV measured with the LHCf experiment

A. Tiberio, on behalf of the LHCf Collaboration
University of Florence and INFN, Florence, Italy

Abstract
The latest physics results of LHCf photon analysis are reported in this paper. The inclusive energy spectrum of photons produced in proton-proton collisions at $\sqrt{s}$ = 13 TeV are shown. The results are compared with the prediction of hadronic interaction models commonly used in air-shower simulations of ultra-high-energy cosmic rays. Even if experimental data lie between the models, there is not a single model consistent with data in all the energy range. The better overall prediction is given by EPOS-LHC hadronic interaction model. The electromagnetic energy flow as a function of pseudorapidity is also presented, showing a good agreement of EPOS-LHC and SIBYLL 2.3 models with data.

Keywords
LHCf; photon; hadronic interaction model; cosmic ray; forward physics.

1 Introduction

The LHC-forward experiment (LHCf) has measured neutral particles production in a very forward region in proton-proton and proton-lead collisions at the Large Hadron Collider. The main purpose of LHCf is to improve hadronic interaction models of Monte Carlo (MC) simulations used in cosmic rays indirect measurements. Highest energy cosmic rays can only be detected from secondary particles which are produced in the interaction of the primary particle with nuclei of the atmosphere, the so-called air showers. Studying the development of air showers, it is possible to reconstruct the type and kinematic parameters of primary particles. To reproduce the development of air showers, MC simulations with accurate hadronic interaction models are needed. Since the energy flow of secondary particles is concentrated in the forward direction, measurements of particle production in the high pseudorapidity region (i.e. small angles) are very important. The energy flow as a function of pseudorapidity is shown in Fig. 1, where also the coverage of LHCf experiment is reported. In the very forward region soft QCD interactions dominates and MC simulations of air showers utilize phenomenological models base on Gribov-Regge theory [1, 2]. Therefore, inputs from experimental data are crucial for the tuning of that models. The LHC accelerator gives the possibility to study a wide range of collision energies, from 0.9 TeV to 13 TeV in the center of mass frame, which corresponds to an energy range in the laboratory frame from 10^{14} eV to 0.9×10^{17} eV. This energy range covers the "knee" region of cosmic rays spectrum, which occurs around 10^{15} eV. Data collected by central detectors with 7 TeV collisions were already used for the tuning of hadronic interaction models widely used in air shower simulations (EPOS-LHC [3], QGSJET II-04 [4] and SIBYLL 2.3 [5]). However, discrepancies between observed data and MC simulations were observed also with these models [6].

2 The detector

LHCf is composed of two independent detectors, called *Arm1* and *Arm2*. Arm1 is located 140 meters away from ATLAS interaction point (IP1) in the IP8 direction, while Arm2 is placed 140 meters away from IP1 in the opposite direction (toward IP2). Detectors are placed inside Target Neutral Absorber (TAN), where the beam pipe turns into two separates tubes. Since charged particles are deviated by the

https://doi.org/10.23727/CERN-Proceedings-2018-001.277

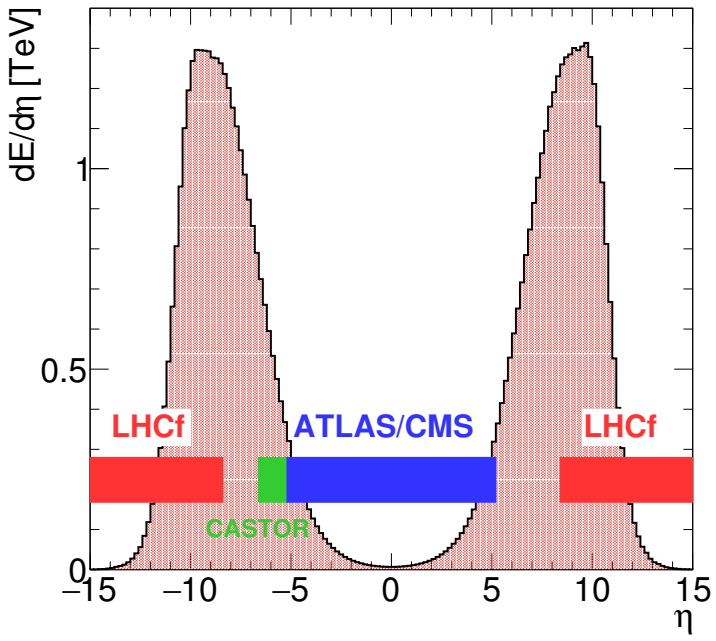

Fig. 1: Pseudorapidity dependence of the energy flow of secondary particles produced in a proton-proton collision at $\sqrt{s}$ = 13 TeV. The coverage of several LHC experiments is also shown.

D1 dipole magnet (which bends colliding beams into the two separate beam pipes), only neutral particles, mainly photons and neutrons, reach the detector.

Each detector is made of two sampling and imaging calorimeters (called *towers* hereafter). Each tower is composed of 16 tungsten layers and 16 scintillator layers to measure the energy deposit and it also contains 4 position sensitive layers. During 0.9 TeV, 2.76 TeV and 7 TeV operations at the LHC, plastic scintillators (EJ-260) were used. Arm1 detector used scintillating fiber (SciFi) to measure position, while Arm2 used silicon microstrip detectors. For 13 TeV operation both detectors were upgraded: all the plastic scintillators were replaced by Gd_2SiO_5 (GSO) scintillators because of their radiation hardness; also the Arm1 SciFi were replaced by GSO bars. In Arm2 the signal of silicon detectors was reduced using a new bonding scheme of the microstrips to avoid saturation of readout electronics due to the higher energy deposit expected at $\sqrt{s} = 13$ TeV.

Transverse cross sections of towers are 20×20 mm^2 and 40×40 mm^2 for Arm1 and 25×25 mm^2 and 32×32 mm^2 for Arm2. Longitudinal dimension of towers is of 44 radiation lengths, which correspond to 1.6 nuclear interaction lengths. Energy resolution is better than 2% for photons above 200 GeV and of about 40% for neutrons. Position resolution for photons is 200 μm and 40 μm for Arm1 and Arm2, respectively, while position resolution for neutrons is of about 1 mm. Smaller tower of each detector is placed on the beam center and covers the pseudo-rapidity range $\eta > 9.6$, while larger tower covers the pseudo-rapidity range $8.4 < \eta < 9.4$. More detailed descriptions of detector performance are reported elsewhere [7–10].

3 Photon analysis results from $\sqrt{s}$ = 13 TeV run

Results for inclusive photon energy spectrum in p-p collisions at $\sqrt{s}$ = 900 GeV and 7 TeV have already been published [11, 12]. Proton-proton collisions at $\sqrt{s} = 13$ TeV were produced for the first time in 2015 at LHC. LHCf had a dedicated low-luminosity run from 9th to 13th of June 2015, with an instantaneous luminosity of $0.3 \div 1.6 \times 10^{29}$cm^{-2}s^{-1}. The data sample used in this analysis was obtained during the LHC Fill #3855 in a 3-hours run started at 22:32 on July 12. The instantaneous luminosity

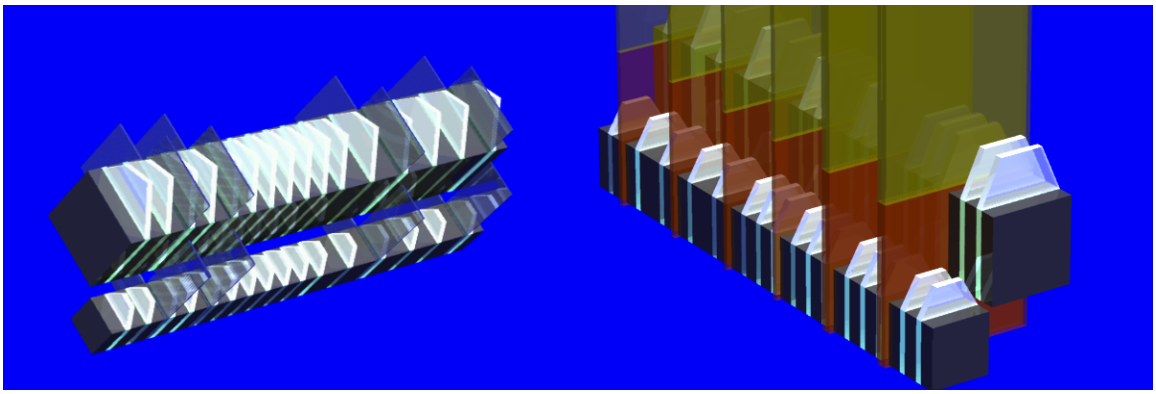

Fig. 2: Schematic view of Arm1 (left) and Arm2 (right) detectors. Tungsten absorbers are shown as dark grey layers and GSO scintillators as cyan layers for both detectors. Blue and red layers represent Arm1 GSO bars and Arm2 silicon detectors, respectively.

(measured by ATLAS [13]) ranged from 3 to 5 $\times 10^{28}$cm^{-2}s^{-1}, with 29 colliding bunches, an half crossing angle of 145 μrad and a β^* of 19 m. The integrated luminosity was 0.191 nb^{-1} for both Arm1 and Arm2, after correcting for data-acquisition live-time. The total inelastic cross section (σ_{inel}) was extrapolated from TOTEM results at 8 TeV using the best fit of σ_{inel} vs $\sqrt{s}$ relation done by the COMPETE collaboration [14, 15].

3.1 Photon inclusive energy spectrum

The inclusive energy spectrum of photon produced in p-p collisions at $\sqrt{s}$ = 13 TeV is presented in Fig. 3 for two pseudo-rapidity ranges together with the predictions of DPMJET 3.06 [16, 17], EPOS-LHC, PYTHIA 8.212 [18, 19], QGSJET II-04 and SIBYLL 2.3 hadronic interaction models. The LHCf data lie between MC predictions but there is not an unique model with a good agreement in the whole energy range and in both rapidity regions. In the pseudorapidity range $\eta > 10.94$, QGSJET and EPOS presents a good overall agreement with experimental data; SIBYLL predicts a lower yield of photons, even if it features a shape similar to data; PYTHIA spectrum agrees with data until ~3.5 TeV but become harder at higher energies; DPMJET is generally harder than data. In the pseudorapidity range $8.81 < \eta < 8.99$, EPOS and PYTHIA spectra agree with data until ~3 TeV, while they become harder at higher energies; SIBYLL has a good agreement until ~ 2 TeV, then also it becomes harder than data; QGSJET presents a lower yield of photons, while DPMJET generally predict an harder spectrum than experimental data. The differences between data and models were attributable to a less-than-complete understanding of the soft hadronic interactions implemented in the models as diffractive processes [20, 21].

3.2 Electromagnetic energy flow

The energy spectrum gives the possibility to calculate the energy flow by integrating the contribution of each energy bin. The analysis was extended to other three pseudorapidity regions of Arm1 detector: $8.52 < \eta < 8.66$, $8.66 < \eta < 8.81$ and $8.99 < \eta < 9.22$. The contribution of each energy bin to the energy flow in shown in Fig. 4: in the regions between $\eta = 8.52$ and $\eta = 9.22$ the dominant contribution comes from low energy photons, while in $\eta > 10.94$ region also high-energy photons matter. The results are compared with the predicted photon energy flow from EPOS, QGSJET and SIBYLL. As can be seen in Fig. 5, data are consistent with EPOS and SIBYLL models near the peak of energy flow, while QGSJET predicts a much lower energy flow. An higher measured flow with respect to all models is found instead for $\eta > 10.94$. The good agreement of data with EPOS and SIBYLL in the peak region is related to the good agreement of the spectrum predicted by these models with data in the low energy region (as shown in Fig. 3 for $8.81 < \eta < 8.99$), which gives the dominant contribution to the energy

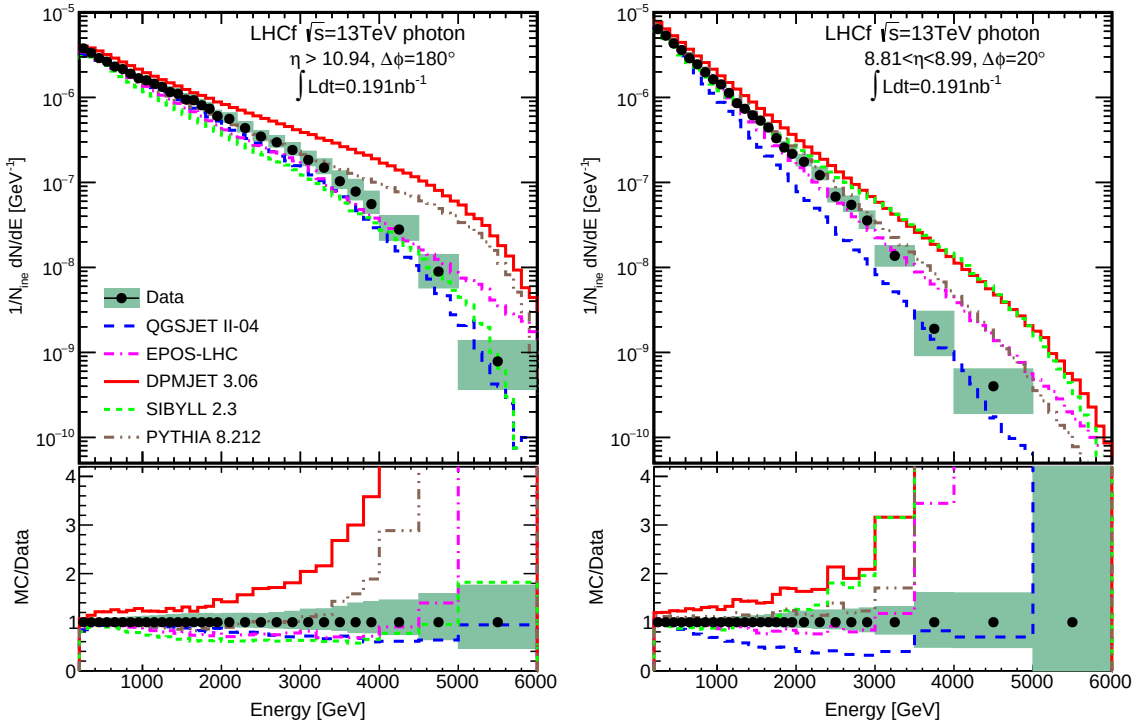

Fig. 3: Inclusive photon energy spectrum for pseudorapidity region $\eta > 10.94$ (left) and $8.81 < \eta < 8.99$ (right). Data are represented by black points while MC prediction from several models are represented by coloured histograms. Green shaded area represents statistical+systematic errors of data. Spectra are normalized to the total number of inelastic collisions. Bottom panels show the ratio of MC predictions to data.

flow.

4 Summary

LHCf experiment performed measurements on very forward photon production in proton-proton collisions at $\sqrt{s}$ = 13 TeV at the LHC accelerator. These measurements are necessary to calibrate hadronic interaction models used in cosmic rays physics to understand the development of atmospheric showers. Measured photon inclusive energy spectrum indicates that there is not an unique model representing the data in the pseudorapidity regions $\eta > 10.94$ and $8.81 < \eta < 8.99$. However, the measured data lie between the prediction of DPMJET, EPOS, PYTHIA, QGSJET and SIBYLL hadronic interaction models. EPOS-LHC model has an overall better agreement with data than other models; QGSJET II-04 has a good agreement in the $\eta > 10.94$ region; PYTHIA 8.212 is consistent with data in the low energy region (below $\sim$3 TeV); SIBYLL 2.3 shows a good agreement below $\sim$2 TeV in the $8.81 < \eta < 8.99$ region; DPMJET 3.06 predicts an harder spectrum than data in both the rapidity regions. The photon energy flow was also calculated form the energy spectrum. Three more pseudorapidity regions were considered in order to study the η dependence of the energy flow. EPOS-LHC and SIBYLL 2.3 show the best agreement with data in the region $8.52 < \eta < 9.22$, while all models predict a lower flow than data in $\eta > 10.94$ region.

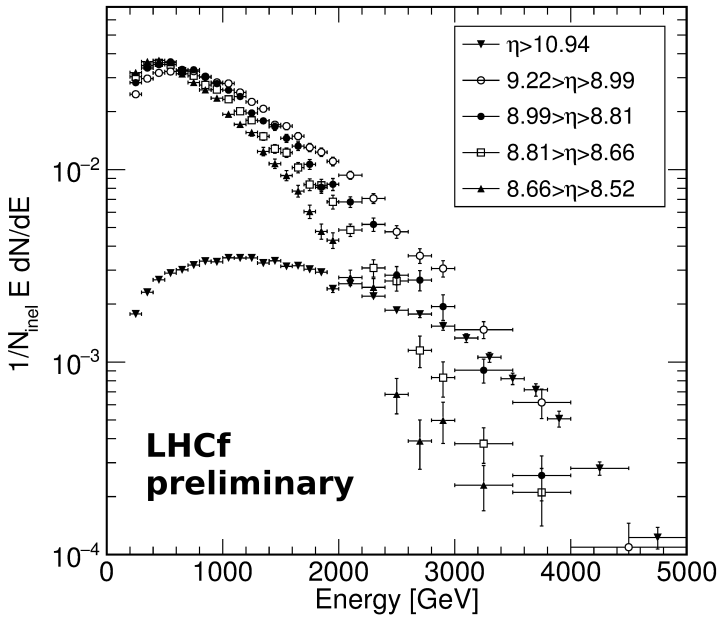

Fig. 4: Electromagnetic energy flow contribution of each energy bin for all pseudorapidity regions of Arm1 detector. In $\eta < 9.22$ regions the main contribution comes from low energy photons.

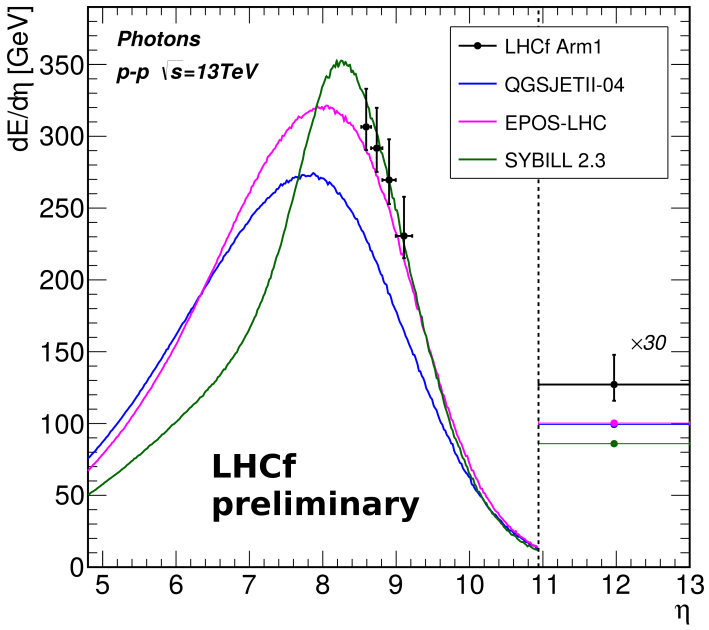

Fig. 5: Electromagnetic energy flow as a function of pseudorapidity. Arm1 data are represented by black points while MC prediction from EPOS-LHC, QGSJET II-04 and SIBYLL 2.3 models are represented by coloured histograms. The point above η = 10.94 is scaled by a factor of 30 for clarity and it is artificially limited to η = 13.

References

[1] V. Gribov, *Sov. Phys. J. Exp. Theor. Phys.* **26**, 414 (1968).
[2] T. Regge, *Nuovo Cimento* **14**, 951 (1959).
[3] K. Werner, F.-M. Liu, and T. Pierog, *Phys. Rev. C* **74**, 044902 (2006).
[4] S. Ostapchenko, *Nucl. Phys. B, Proc. Suppl.* **151**, 143 (2006).
[5] F. Riehn, Felix *et al.*, *PoS ICRC2015* (2016) 558.
[6] The Pierre Auger Collaboration, *PRL* **117** (2016) 192001.
[7] O. Adriani *et al.*, *JINST* **3**, S08006 (2008).
[8] O. Adriani *et al.*, *JINST* **5**, P01012 (2010).
[9] Y. Makino, A. Tiberio *et al.*, 2017 *JINST* **12** P03023.
[10] K. Kawade *et al.*, *JINST* **9**, P03016 (2014).
[11] O. Adriani *et al.*, *Physics Letters B* **703**, 128-134 (2011).
[12] O. Adriani *et al.*, *Physics Letters B* **715**, 298-303 (2012).
[13] ATLAS collaboration, *Eur. Phys. J. C* **76** (2016) 653.
[14] G. Antchev *et al.*, *Phys. Rev. Lett.*, vol. **111**, p. 012001, Jul 2013.
[15] K. A. Olive *et al.*, *Chin. Phys.*, vol. **C38**, p. 090001, 2014.
[16] F. W. Bopp, J. Ranft, R. Engel, and S. Roesler, *Phys. Rev. C* **77**, 014904 (2008).
[17] R. Engel, J. Ranft, and S. Roesler, *Phys. Rev. D* **55**, 6957 (1997).
[18] T. Sjöstrand, S. Mrenna, and P. Skands, *J. High Energy Phys.* **05** (2006) 026.
[19] T. Sjöstrand, S. Mrenna, and P. Skands, *Comput. Phys. Commun.* **178**, 852 (2008).
[20] S. Ostapchenko, *Phys. Lett. B* **703** (2011) 588592
[21] Q. D. Zhou *et al.*, *Eur. Phys. J. C* **77** (2017) no.4, 212